

Anomalous phase behavior in a model fluid with only one type of local structure

Santi Prestipino¹ [*], Franz Saija² [†], and Gianpietro Malescio¹ [‡]

¹ *Università degli Studi di Messina, Dipartimento di Fisica,
Contrada Papardo, 98166 Messina, Italy*

² *CNR-Istituto per i Processi Chimico-Fisici,
Viale Ferdinando Stagno d'Alcontres 37, 98158 Messina, Italy*

(Dated: February 23, 2024)

Abstract

We present evidence that the concurrent existence of two populations of particles with different effective diameters is not a prerequisite for the occurrence of anomalous phase behaviors in systems of particles interacting through spherically-symmetric unbounded potentials. Our results show that an extremely weak softening of the interparticle repulsion, yielding a single nearest-neighbor separation, is able to originate a wide spectrum of unconventional features including reentrant melting, solid polymorphism, as well as thermodynamic, dynamic, and structural anomalies. These findings extend the possibility of anomalous phase behavior to a class of systems much broader than currently assumed.

PACS numbers: 61.20.Ja, 62.50.-p, 64.70.D-

Keywords: anomalous melting, solid-solid transition, high-pressure phase diagrams of the elements

I. INTRODUCTION

The phase behavior of one-component substances is termed “anomalous” whenever it differs from that of prototypical (i.e., argon-like) liquids. Anomalous phase behavior includes polymorphism in the liquid and solid phases, reentrant melting (i.e., melting by compression at constant temperature), and a host of other thermodynamic, dynamic, and structural anomalies. An important class of systems displaying such features is that of network-forming fluids, i.e., fluids that form orientation-specific, intermolecular bonds which are strong relative to London forces. The most well-known of these substances is water [4, 5], while other cases are silicon, phosphorous, and silica [6–8]. Anomalous behaviors have been observed also in systems where effective interatomic forces can reasonably be assumed non-directional. For example, alkali and alkali-earth metals at high pressures exhibit one or more regions of reentrant melting [9]. Liquid or amorphous polymorphism have been found in other systems with non-directional interactions, such as molten $\text{Al}_2\text{O}_3\text{-Y}_2\text{O}_3$ [10], triphenyl phosphite [11], and some metallic glasses [12].

The quest for understanding the basic mechanisms of anomalous phase behaviors has given impulse to the study of simple isotropic potentials that are able to display the same behaviors. These systems can be appropriate models for the generic thermodynamic behavior of pure metals, metallic mixtures, electrolytes, and colloids. It has been found that unusual behaviors may arise in systems of spherical particles (simple fluids) where the unbounded repulsive core is “softened” through the addition of a finite repulsion at intermediate distances, so as to generate two distinct length scales in the system: a “hard” one, related to the inner core, and a “soft” one, associated with the soft, penetrable, component of the repulsion [13–26]. Due to this feature, such core-softened (CS) fluids are characterized by two competing, expanded and compact, local arrangements of particles. This property mimics the behavior of the more complex network-forming fluids, where loose and compact local structures arise from the continuous formation and disruption of the dynamic network originated by orientational bonds. So far, the existence of two competing local structures has been regarded as essential for the occurrence of anomalous phase behaviors in simple fluids. In this work we challenge this belief and provide evidence that these behaviors may also occur in systems with a single local particle arrangement, i.e., under much weaker conditions than admitted so far.

II. THEORY AND SIMULATION

For a spherically-symmetric unbounded potential $u(r)$ the analytic condition for core softening [27] is that, in a range of interparticle distances r within the core, the product $rf(r)$, with $f(r) = -du/dr$, decreases as r gets smaller. Systems satisfying this core-softening condition are characterized by two different repulsive length scales and, for pressures where the two scales are both effective, loose and compact local arrangements compete with each other and the fluid behaves like a mixture of two particle species with different radii (“two-state” fluid [28–30]). A typical property of such fluids is the existence of a reentrant melting line, a feature that is strictly related to other anomalous behaviors [29]. We note that the core-softening condition is not applicable to lattice models with a softened two-body repulsion, which can nonetheless show a reentrant-melting behavior [31, 32].

In order to assess whether or not the existence of two distinct local structures is a necessary requirement for reentrant melting, we ask the following question: how much soft should repulsion be in order that reentrant melting may occur in simple fluids? To attempt an answer, we have developed a convenient tool for the analysis of trends in the melting-line topology, based on linear-elasticity theory [33]. We focus on the face-centered cubic (fcc) and the body-centered cubic (bcc) phases, i.e., those relevant for purely-repulsive potentials at low to moderate pressure. According to elasticity theory, the enthalpy of a cubic-symmetry solid under homogeneous strain is

$$H = H_0 + V_0 \left\{ \frac{1}{2} \lambda_1 (e_{xx}^2 + e_{yy}^2 + e_{zz}^2) + \lambda_2 (e_{xx}e_{yy} + e_{xx}e_{zz} + e_{yy}e_{zz}) + 2\lambda_3 (e_{xy}^2 + e_{xz}^2 + e_{yz}^2) \right\}, \quad (1)$$

where H_0 is the enthalpy of the undeformed crystal with volume V_0 , $e_{\alpha\beta}$ are the strain-tensor components, and the λ 's are Lamé coefficients. At zero temperature, these coefficients are given in terms of the interparticle potential [34], being ultimately a function of pressure. Then, we employ Eq. (1) in a field theory where the field variables are the components of the displacement vector $\mathbf{d}(\mathbf{R})$ at each lattice site. In practice, any given realization of the displacement field is assigned the weight $\exp\{-H/(k_B T)\}$, with the λ 's fixed at their $T = 0$ values. In Fourier space, this eventually gives the mean square displacement as a Gaussian integral. We find

$$\langle d^2 \rangle = k_B T \int_{\text{DS}} \frac{d^3 q}{(2\pi)^3} \text{Tr}[M^{-1}(\mathbf{q})], \quad (2)$$

where the sum in (2) is over the Debye sphere (DS) and $M^{-1}(\mathbf{q})$ is the inverse of

$$M_{\alpha\beta}(\mathbf{q}) = [\lambda_3 q^2 + (\lambda_1 - \lambda_2 - 2\lambda_3) q_\alpha^2] \delta_{\alpha\beta} + (\lambda_2 + \lambda_3) q_\alpha q_\beta. \quad (3)$$

Derivation of Eq.(2) assumes that the quadratic form in (1) is positive definite, meaning that the stability conditions $\lambda_1 + 2\lambda_2 > 0$, $\lambda_1 - \lambda_2 > 0$, and $\lambda_3 > 0$ must hold. At those pressures where any of these inequalities fails to be satisfied, the solid is mechanically unstable.

We obtain a closed-form expression for the melting temperature $T_m(P)$ by using Lindemann's criterion, i.e., by equating the r.h.s. of Eq.(2) for $T = T_m$ to $(\delta_L r_{\text{NN}})^2$, where $\delta_L \approx 0.15$ for a fcc solid and $\delta_L \approx 0.18$ for a bcc solid [35], and r_{NN} is the nearest-neighbor (NN) distance. We have checked in known cases (Lennard-Jones, exp-6, and Gaussian potentials) that the present criterion correctly predicts the overall trend of the fcc and bcc melting lines, although T_m is systematically overestimated, which is not surprising in view of the assumption of temperature-independent λ 's.

We now apply the above outlined melting criterion to two different types of repulsive interactions with tunable softness. We first consider the modified inverse-power (MIP) potential $u_{\text{MIP}}(r) = u_0(r)[1 + A \exp\{-10(1 - r/\sigma)^2\}]$ with $u_0(r) = \epsilon(r/\sigma)^{-6}$, ϵ and σ being energy and length units. As $|A|$ increases, core repulsion becomes softer and the core-softening condition is satisfied for $A \lesssim -0.60$ and $A \gtrsim 28$. Our criterion predicts reentrant melting for $A \lesssim -0.35$ (Fig. 1) and $A \gtrsim 1$ (not shown). We perform similar calculations for a different interaction law, $u_{\text{YK}}(r) = \epsilon \exp\{a(1 - r/\sigma) - 6(1 - r/\sigma)^2 \ln(r/\sigma)\}$, introduced long ago by Yoshida and Kamakura (YK) [36]. This repulsion becomes softer with decreasing a and satisfies the core-softening condition for $a \lesssim 2.3$. The theoretical melting line shows a reentrant portion for $a \lesssim 5.5$ (see Fig. 2).

The above results intriguingly suggest that reentrant melting (and presumably also other anomalous behaviors) can occur for continuous potentials that *do not* satisfy the core-softening condition. To assess this possibility, we investigate through numerical simulation the equilibrium properties of a system of particles interacting through $u_{\text{YK}}(r)$ for $a = 3.3$. This potential does not satisfy the core-softening condition and monotonously increases, for decreasing r , together with its first and second derivatives (see Fig. 3 inset). To carry on the simulation study, we assume that the same crystals that are stable at $T = 0$ also give the underlying lattice structure for the stable solid phases at $T > 0$. Through a total-energy calculation similar to that in [37], we find that at $T = 0$ the sequence of stable crystals for

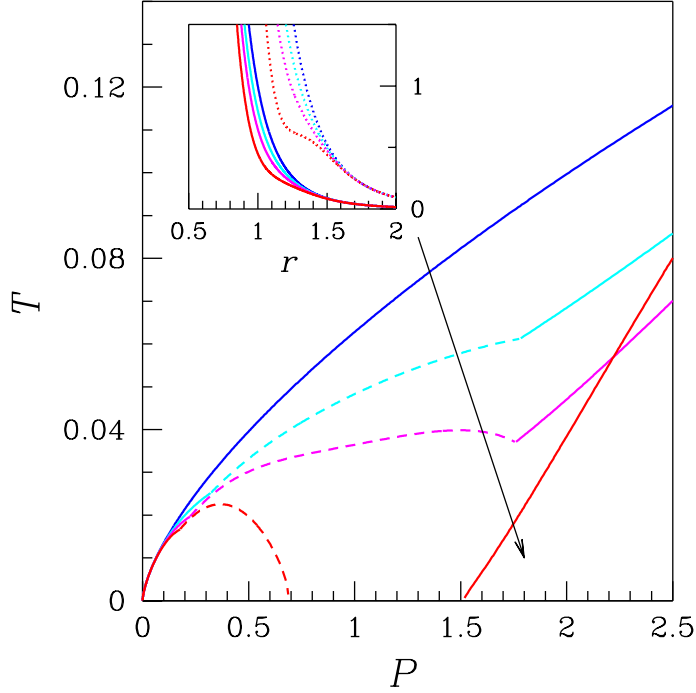


FIG. 1: (Color online). Theoretical melting lines (see text) for $u_{\text{MIP}}(r)$. Pressure P and temperature T are in reduced, ϵ/σ^3 and ϵ/k_B , units. Melting lines are obtained by taking, for each P , the higher T_m value between fcc (solid line) and bcc (dashed line). Four cases are shown: $A = 0$ (blue), -0.2 (cyan), -0.35 (magenta), -0.55 (red). Repulsion softness grows in the arrow direction. Cusps at estimated fluid-fcc-bcc triple points are artefacts of the approximation. Upon increasing the repulsion softness further and further, a stability gap eventually opens at $T = 0$ for both fcc and bcc solids, which will be filled by one or more low-coordinated crystals. In the inset, the four potentials are plotted as continuous lines, with the respective $rf(r)$ also shown as dotted lines.

increasing pressures is (see [37] for acronyms)

$$\text{fcc} \xrightarrow{0.66} \text{bcc} \xrightarrow{2.51} \beta\text{Sn} \xrightarrow{3.50} \text{sh} \xrightarrow{3.86} \text{sc} \xrightarrow{5.07} \beta\text{Sn} \xrightarrow{7.22} \text{cI16} \xrightarrow{8.33} \text{fcc} \xrightarrow{16.7} \text{hcp} \xrightarrow{64.8} \text{fcc} \xrightarrow{282} \text{hcp} \xrightarrow{518} \text{fcc}, \quad (4)$$

where the numbers are the transition pressures in units of ϵ/σ^3 . We note that the internal parameter of the stable cI16 crystal varies from 0.043 to 0.047, incidentally close to the cI16 phases of Li [38] and Na [39].

We have performed extensive Monte Carlo (MC) and molecular-dynamics simulations, using samples of 500 to 800 particles (simulations with 2048 particles lead to practically the

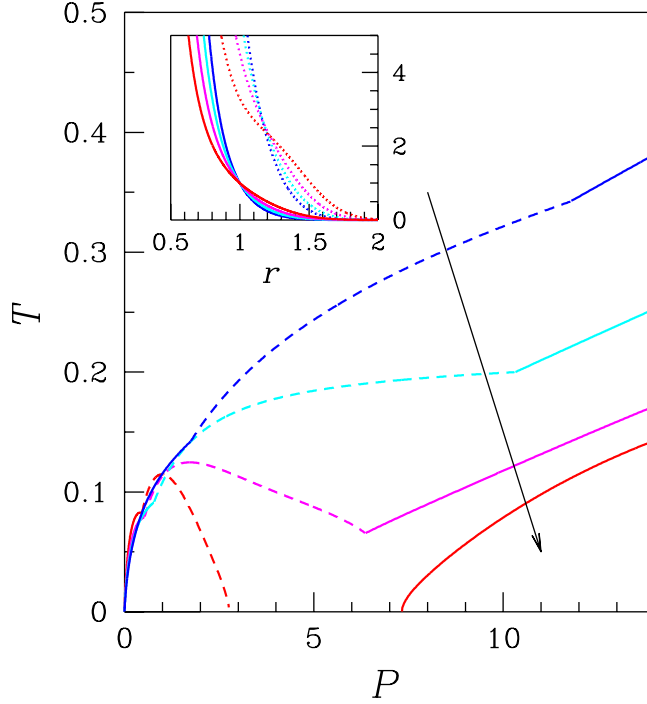


FIG. 2: (Color online). Theoretical melting lines (see text) for $u_{\text{YK}}(r)$. Four cases are shown: $a = 6.9$ (blue), 5.7 (cyan), 4.5 (magenta), 3.3 (red). Repulsion softness grows in the arrow direction. Upon increasing the repulsion softness further and further, a stability gap eventually opens at $T = 0$ for both fcc and bcc solids, which will be filled by one or more low-coordinated crystals. In the inset, the four potentials are plotted as continuous lines, with the respective $rf(r)$ also shown as dotted lines.

same results). Coexistence lines are computed by exact free-energy methods (details of the MC simulation are as in [25]). The phase diagram for $P < 3$ is plotted in Fig. 3. The bcc melting temperature shows a maximum at $P \simeq 0.75$, hence at not too low temperatures the bcc solid melts upon compression into a denser fluid. At still lower temperatures, the bcc phase transforms into a βSn phase. In the reentrant-fluid region a density anomaly occurs, i.e., the number density decreases upon cooling at constant pressure. This region is bounded from above by the temperature of the maximum density line (see Fig. 3). In Fig. 3, we also show points of diffusivity minimum and of $-s_2$ maximum, s_2 being the two-body entropy [40]. Similarly to water, the region of structural anomaly encompasses that of anomalous diffusion, which in turn encloses the region of density anomaly. A compendium

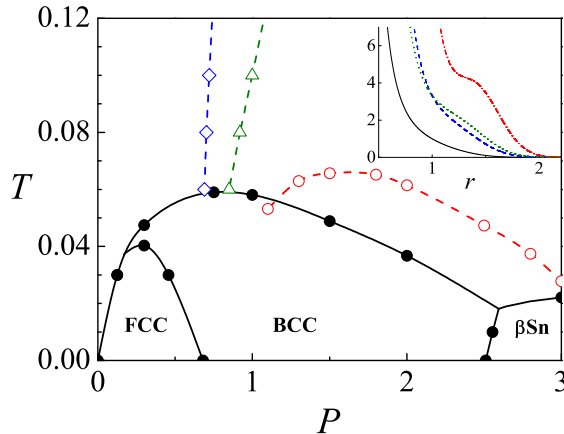


FIG. 3: (Color online). Phase diagram of the YK potential for $a = 3.3$ (P and T are in reduced units). Full dots are two-phase coexistence points. Open dots are points of density maximum in the fluid phase. Diamonds and triangles denote points of $-s_2$ maxima and D minima respectively (D being the self-diffusion coefficient), giving the left boundary of the regions of structural and diffusion anomaly (the right boundaries, defined by $-s_2$ minima and D maxima, are out of the P range shown). Numerical errors are smaller than the symbols size. Within the pressure range $2.5 \div 3$, the aspect ratio of the βSn phase is $c/a \simeq 0.60$. Inset: $u_{\text{YK}}(r)$ for $a = 3.3$ (black solid line), $f(r) = -u'_{\text{YK}}(r)$ (blue dashed line), $rf(r)$ (green dotted line), $u''_{\text{YK}}(r)$ (red dot-dashed line).

of the anomalous behavior of the present system is shown in Fig. 4.

III. DISCUSSION

The anomalies exhibited by the YK fluid for $a = 3.3$ are quite similar to those of CS potentials. However, the much weaker softness of the former leads to peculiar local arrangement of particles in the fluid phase, as evidenced in the radial distribution function $g(r)$. As P increases at constant temperature, the NN peak of $g(r)$ moves gradually toward small r (Fig. 5, top panel). Meanwhile its height first grows, due to increasing proximity with the bcc solid, and then goes down in the pressure range where reentrant melting occurs. As P increases further, the NN peak of $g(r)$ grows again while its position changes less and less sensibly due to the steep small- r repulsion. At low pressures, the behavior of $g(r)$ is

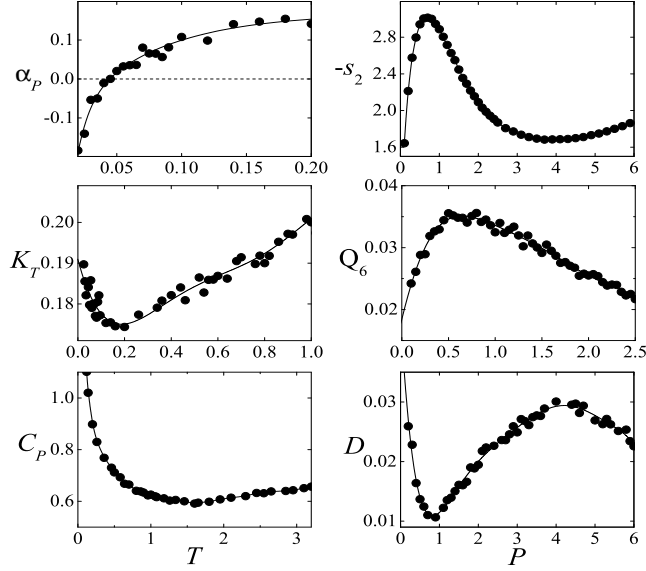


FIG. 4: Thermodynamic and structural quantities for the YK fluid with $a = 3.3$. Left column: thermal expansion coefficient α_P (units of k_B/ϵ), isothermal compressibility K_T (units of σ^3/ϵ), and constant-pressure specific heat C_P (units of k_B) as a function of T along the isobar $P = 2.5$. For conventional liquids, α_P , K_T , and C_P monotonically increase with T and $\alpha_P > 0$. Right column: translational order parameter $-s_2$ (units of k_B), bond-order parameter Q_6 [41], and self-diffusion coefficient D (units of $\sigma(\epsilon/m)^{1/2}$, where m is particle mass) as a function of P along the isotherm $T = 0.06$. For conventional liquids, $-s_2$ and Q_6 increase with P while D decreases monotonically.

similar to that of the Gaussian-core model [42] (GCM), a fluid with a bounded interaction potential that also exhibits a bunch of waterlike anomalies. However, due to the absence of a true particle core, the behavior is completely different at high pressures where the GCM more and more resembles an “infinite-density ideal gas” with a radial distribution function $g(r) = 1$. To our knowledge, the $g(r)$ behavior of the system investigated here has never been reported for other systems of truly impenetrable particles.

To make clear the difference between the interaction studied here and the CS potentials investigated so far, we report the radial distribution function of a CS potential (Fig. 5, bottom panel). In this case, the heights of the first two peaks of $g(r)$, associated respectively with the hard and soft length scales, change in opposite directions on increasing pressure, signalling that the “hard” NN distance becomes more and more populated at the expenses of

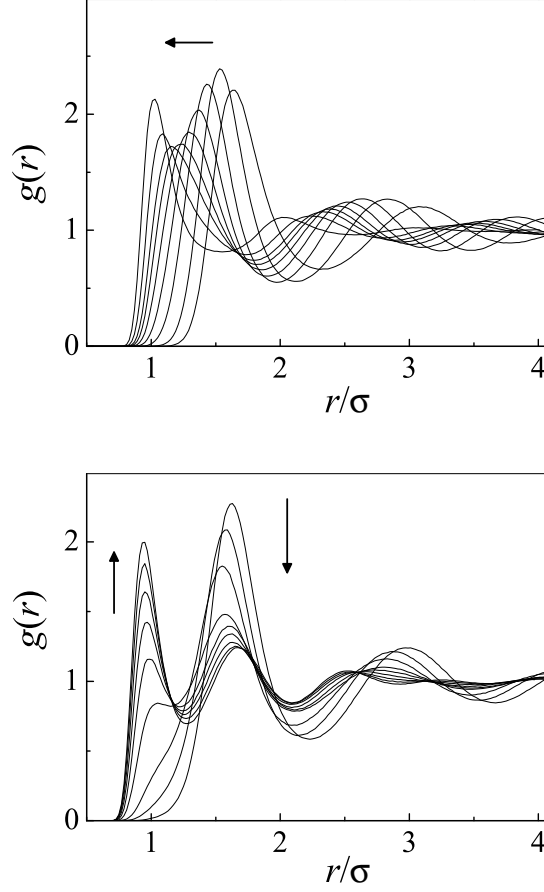


FIG. 5: Top panel: pair distribution function $g(r)$ of the YK potential for $a = 3.3$. Bottom panel: $g(r)$ of the YK potential for $a = 2.1$ (not far from the core-softening threshold $a = 2.3$). For $a = 3.3$, lines correspond to $T = 0.06$ and $P = 0.1, 0.5, 1, 1.5, 2, 2.5, 3, 4, 6$. For $a = 2.1$, curves refer to $T = 0.07$ and $P = 0.5, 0.7, 1, 1.6, 2.3, 3, 4.1, 5.2, 6.4$. The arrows mark the direction of pressure increase.

the “soft” distance, while the position of the two peaks remains essentially unaltered. This behavior is a clear evidence of the simultaneous existence of two populations of particles having distinct effective diameters, a phenomenon that does not occur in the case analyzed here.

To gain further insight we analyze the P dependence of the NN peak position r_{NN} for the system under study, as compared with a CS potential ($u_{\text{YK}}(r)$ with $a = 2.1$) and $u_0(r)$ (see Fig. 6). For the CS potential, $r_{\text{NN}}(P)$ consists of two branches, i.e., in a range of

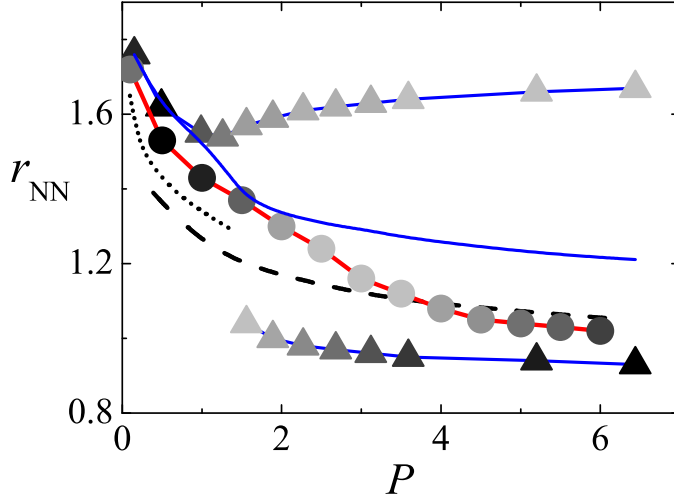


FIG. 6: Position r_{NN} of the NN peak of $g(r)$ in units of σ as a function of P at constant T for: $u_{\text{YK}}(r)$, $a = 2.1$ and $T = 0.07$ (blue solid line and triangles); $u_{\text{YK}}(r)$, $a = 3.3$ and $T = 0.06$ (red solid line and full dots); $u_0(r)$, $T = 0.06$ (black dotted line, stopping near the melting point); $u_0(r)$, $T = 1$ (black dashed line). The gray scale is proportional to the height of the $g(r)$ peak. The blue solid line without symbols represents a weighted average of the two r_{NN} branches, with weights proportional to the respective $g(r)$ peak heights, for the case $u_{\text{YK}}(r)$ with $a = 2.1$.

pressures two distinct populations of particles with different effective radii coexist, which legitimates the two-state-fluid picture. On the contrary, for the present system $r_{\text{NN}}(P)$ has only one branch (similarly to $u_0(r)$ where, however, the $g(r)$ peaks grow monotonously with P), meaning that all particles have the same effective radius. While the $r_{\text{NN}}(P)$ curve for $u_0(r)$ is upward concave everywhere, in the present case it shows a portion with downward concavity, roughly corresponding to the reentrant-melting pressure range. The same feature is displayed by the weighted average of the two r_{NN} branches for the CS potential (the downward-concave region is here shifted, as well as the reentrant portion of the melting line, towards smaller pressures).

Thus, in the case considered here there exists only one type of local structure with an effective length scale that, however, shrinks with pressure in such a way as to capture the P -dependence of the mean length scale for the CS case. In particular, the shrinking rate shows a local maximum in the reentrant-melting pressure range, which makes the length

scale more loosely defined with respect to the adjacent regions. As shown by our results, this is sufficient to give origin to anomalous phase behavior.

IV. CONCLUDING REMARKS

Competition between two different local particle arrangements, arising from either directional or core-softened isotropic forces, has so far deemed to be responsible for anomalous thermodynamic behavior. In this article, we have shown that the same behaviors may occur also for weakly-softened (WS) potentials, i.e., simple fluids characterized by a repulsion that is only marginally softened and yields a single structure at a local level. Our results overturn the two-state-fluid picture derived from network-forming fluids and simplify the minimal scenario for the occurrence of anomalous behaviors, thus considerably widening the class of interactions that give rise to waterlike anomalies. WS potentials can be relevant in the realm of soft matter, where engineering interparticle forces is possible, and also for “hard” matter under extreme conditions. In the latter case, pressure typically induces successive rearrangements of the crystal structure in order to minimize the electronic energy. This is reflected at higher T in reentrant melting and (though more rarely reported [43]) waterlike anomalies. The effect of pressure on the atomic structure may be dramatic, like e.g. in Cs where a 6s-5d band crossing causes a sudden drop in the effective radius of the atom [44] (“orbital collapse”), or less sharp as can be expected for lighter and smaller chemical elements. While two-scale CS potentials offer a simple model for systems undergoing orbital collapse, one-scale WS potentials may be appropriate to describe those elements where the atomic radius shrinks more gradually under pressure.

[*] E-mail: `sprestipino@unime.it`

[†] Corresponding author. E-mail: `saija@me.cnr.it`

[‡] E-mail: `malescio@unime.it`

[4] P. G. Debenedetti *Metastable Liquids* (Princeton University Press, Princeton, 1996).

[5] O. Mishima and H. E. Stanley, *Nature* **396**, 329 (1998).

[6] S. Sastry and C. A. Angell, *Nature Mater.* **2**, 739 (2003).

[7] Y. Katayama *et al.*, *Nature* **403**, 170 (2000).

- [8] C. Meade *et al.*, Phys. Rev. Lett. **69**, 1387 (1992).
- [9] D. A. Young, *Phase Diagrams of the Elements* (University of California, Berkeley, 1991).
- [10] S. Aasland and P. F. McMillan, Nature **369**, 633 (1994).
- [11] H. Tanaka *et al.*, Phys. Rev. Lett. **92**, 025701 (2004).
- [12] H. W. Sheng *et al.*, Nature Materials **6**, 192 (2007).
- [13] P. C. Hemmer and G. Stell, Phys. Rev. Lett. **24**, 1284 (1970).
- [14] M. R. Sadr-Lahijany *et al.*, Phys. Rev. Lett. **81**, 4895 (1998).
- [15] E. A. Jagla, Phys. Rev. E **58**, 1478 (1998).
- [16] M. Watzlawek *et al.*, Phys. Rev. Lett. **82**, 5289 (1999).
- [17] G. Franzese *et al.*, Nature **409**, 692 (2001).
- [18] Z. Yan *et al.*, Phys. Rev. Lett. **95**, 130604 (2005).
- [19] H. M. Gibson and N. B. Wilding, Phys. Rev. E **73**, 061507 (2006).
- [20] G. Malescio, J. Phys.: Condensed Matter **19**, 073101 (2007)
- [21] D. Yu. Fomin *et al.*, J. Chem. Phys. **129**, 064512 (2008).
- [22] G. J. Pauschenwein and G. Kahl, Soft Matter **4**, 1396 (2008).
- [23] G. Malescio *et al.*, J. Chem. Phys. **129**, 241101 (2008).
- [24] A. B. de Oliveira *et al.*, Europhys. Lett. **85**, 36001 (2009).
- [25] F. Saija *et al.*, Phys. Rev. E **80**, 031502 (2009).
- [26] E. Lascaris *et al.*, Phys. Rev. E **81**, 031201 (2010).
- [27] P. G. Debenedetti *et al.*, J. Phys. Chem. **95**, 4540 (1991).
- [28] E. Rapoport, J. Chem. Phys. **46**, 2891 (1967).
- [29] P. F. McMillan, J. Mater. Chem. **14**, 1506 (2004).
- [30] P. G. Debenedetti and H. E. Stanley, Physics Today **56**, 40 (2003).
- [31] J. S. Høye *et al.*, Mol. Phys. **107**, 321 (2009).
- [32] N. G. Almarza *et al.*, J. Chem. Phys. **131**, 124506 (2009).
- [33] See e.g. T. H. K. Barron and M. L. Klein, Proc. Phys. Soc. **85**, 523 (1965).
- [34] M. C. Rechtsman *et al.*, Phys. Rev. Lett. **101**, 085501 (2008).
- [35] F. Saija *et al.*, J. Chem. Phys. **124**, 244504 (2006).
- [36] T. Yoshida and S. Kamakura, Prog. Theor. Phys. **52**, 822 (1974).
- [37] S. Prestipino *et al.*, Soft Matter **5**, 2795 (2009).
- [38] M. Hanfland *et al.*, Nature **408**, 174 (2000).

- [39] M. I. McMahon *et al.*, Proc. Natl. Acad. Sci. USA **104**, 17297 (2007).
- [40] See e.g. R. Esposito *et al.*, Phys. Rev. E **73**, 040502(R) (2006).
- [41] P. J. Steinhardt *et al.*, Phys. Rev. B **28**, 784 (1983).
- [42] C. N. Likos, Phys. Rep. **348**, 267 (2001).
- [43] H. Thurn and J. Ruska, J. Non-Cryst. Solids **22**, 331 (1976).
- [44] R. Sternheimer, Phys. Rev. **78**, 235 (1950).